Supplementary Information (SI) for New Journal of Chemistry.
This journal is © The Royal Society of Chemistry and the Centre National de la Recherche Scientifique 2024

Supporting Information

Stable P3HT-PC_{61}BM inverted organic solar cells based on cerium oxide as electron transport layer

Sana Abidi,[a,b] Amir Hossein Habibi,[a] Hayley Melville,[a] Sylvie Dabos-Seignon,[a] Olivier Segut,[a] Tony Breton,[a] Eric Levillain,[a] Clément Cabanetos,[a] Saad Touihri,[b*] and Philippe Blanchard[a*]

[a] Univ Angers, CNRS, MOLTECH-ANJOU, SFR MATRIX, F-49000 Angers, France. [b] Laboratoire Nanomatériaux, Nanotechnologie et Energie (L2NE), University of Tunis el Manar, Tunisia.

Corresponding authors: philippe.blanchard@univ-angers.fr; saad.touihri@ensit.rnu.tn

Table of contents:

1. General methods
2. X-ray photoelectron spectroscopy (XPS)
3. Transmittance measurements and determination of optical bandgaps E_g
4. Contact angle measurements
5. Absorption spectra of the P3HT:PC61BM photoactive layer
6. AFM analysis of the P3HT:PC_{61}BM photoactive layer
7. PESA measurements and determination of ionization energies
8. AFM analysis of CeO_x layers
9. Evaluation of device stability
10. References

1. General methods

UV-vis spectra were recorded on a Shimadzu UV-1800 spectrometer (Shimadzu, Kyoto, Japan). Infrared spectra were recorded on a Bruker spectrometer Vertex 70. Thermogravimetric analysis (TGA) measurements were performed with a TA Instruments Q500 with a ramp of 10 °C/min under a nitrogen flow. Photoelectron spectroscopy in air (PESA) was carried out on a Riken AC-2 photoelectron spectrometer (Riken Keiki, Tokyo, Japan). Thin-film X-ray diffraction (XRD) analysis which was measured on a D8 Bruker diffractometer (Cu Kα, λ = 1.5418 Å) equipped with a linear Vantec super speed detector. X-ray photoelectron spectroscopy (XPS) analyses were recorded on a Kratos Axis Ultra spectrometer and the X-ray source employed was monochromated Al Kα source operating at 1486.6 eV. Atomic force microscopy (AFM) experiments were performed using the Nano-Observer device from CS Instrument. Images were processed with the Gwyddion free SPM data analysis software. The thickness of layer was measured using a KLA Tencor-D500 optical profilometer. Measurements of contact angles of liquid droplets were carried out with a contact angle goniometer from Ossila.

2. X-ray photoelectron spectroscopy (XPS)

XPS data were acquired using a Kratos Axis Ultra spectrometer. The X-ray source employed was monochromated Al Kα source operating at 1486.6 eV. Spectra were collected at a take-off angle of 90°, using a spot size of 0.7×0.3 mm^2 at a pressure below 10-8 mbar. High-resolution scans were performed with a step size of 0.1 eV and a pass energy of 40 eV. Calibration was done using C1s as a reference, with a binding energy of 284.5 eV, without the need for an internal standard. XPS spectra were analyzed using the curve-fitting software CASA XPS. The background subtraction was performed using the U2 Tougaard method, followed by fitting the peaks using a pseudo-Voigt function that combined Gaussian and Lorentzian functions.

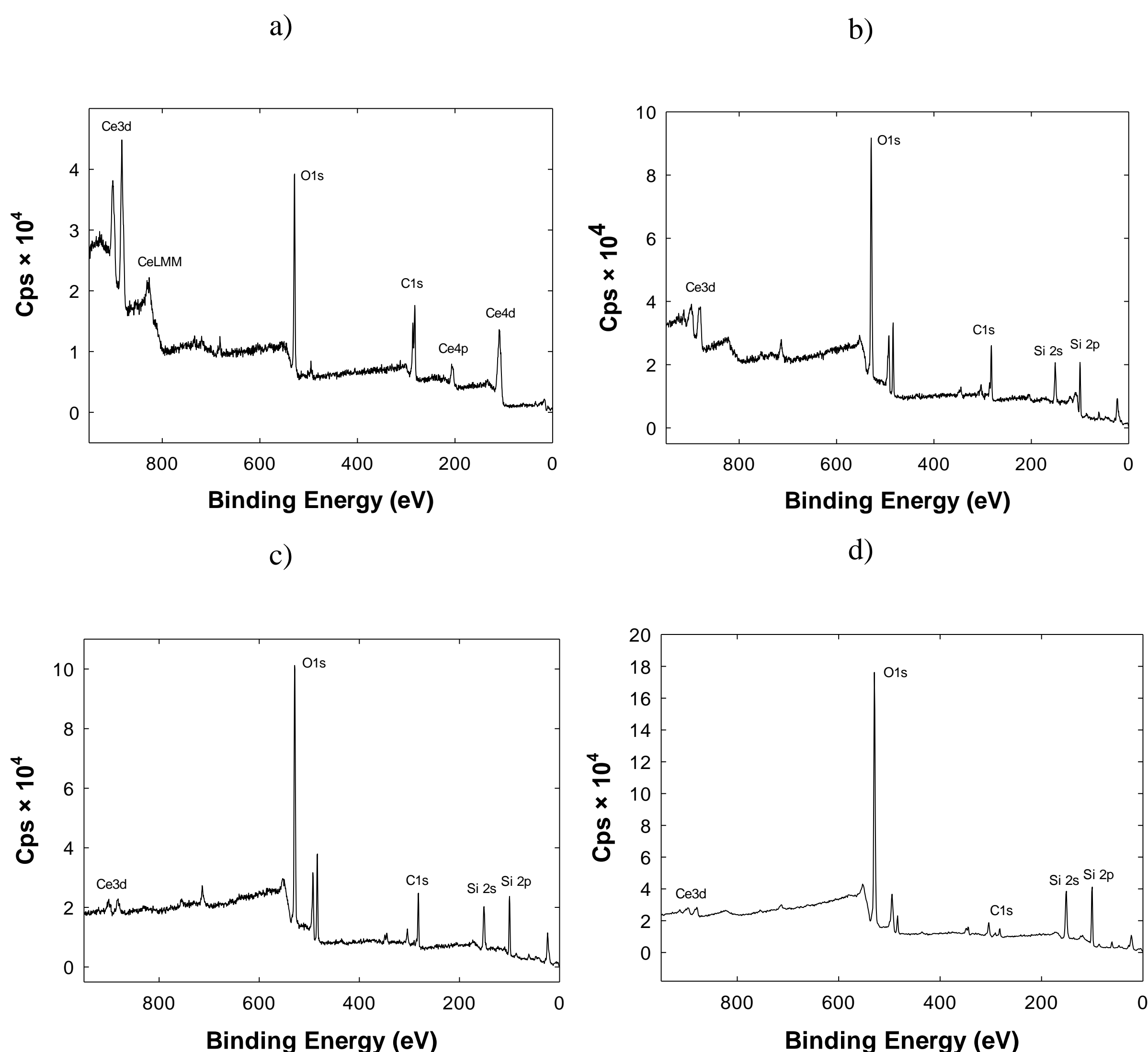

Figure S1. Full XPS spectra of cerium(III) acetate (a), thin films of the CeO_x precursor without TA (b), and after treatment at 200°C (c) or 450°C (d) for 15 min.

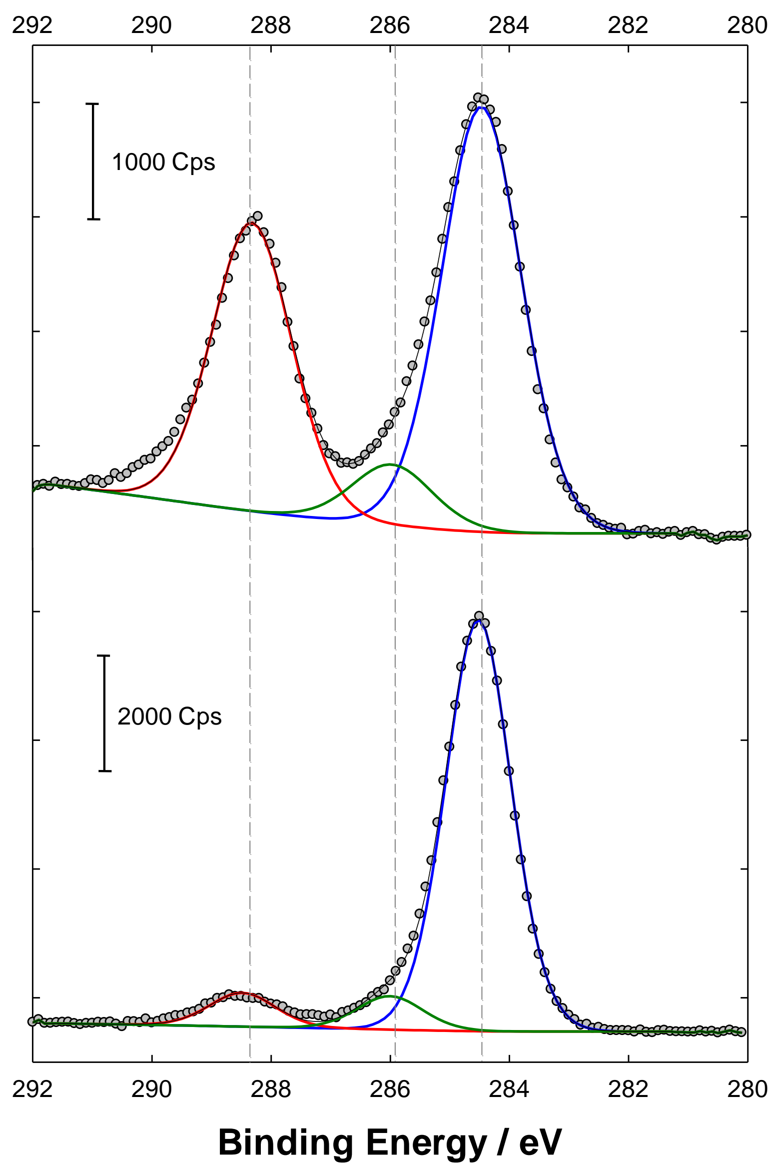

Figure S2. Carbon 1s XPS core-level spectra of cerium(III) acetate as powder (top) and a thin film of the CeO_x precursor without TA (bottom).

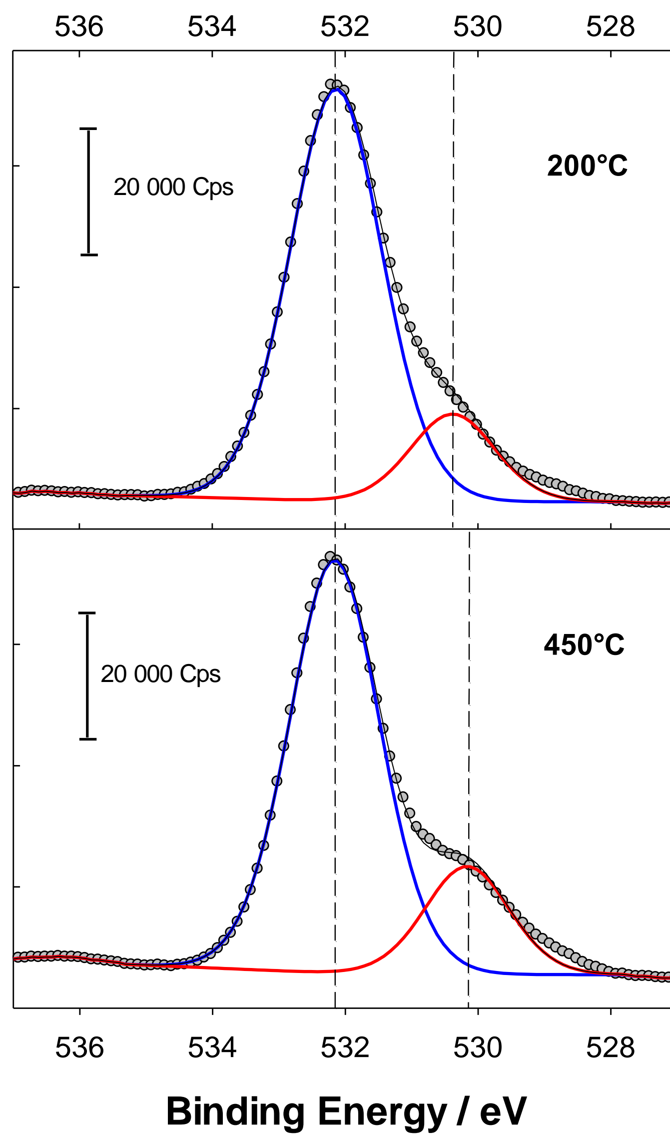

Figure S3. Oxygen 1s XPS core-level spectra of thin films of the CeO_x precursor after treatment at 200°C (top) or 450°C (bottom) for 15 min.

3. Transmittance measurements and determination of optical bandgaps E_g

The transmission spectra of ZnO and CeO_x thin films are shown in Figure X. The band energies of ZnO and CeO_x were measured using the Tauc method according to the following equation:[1]

$$\alpha h\upsilon = B(h\upsilon - E_g)^{\frac{1}{2}},$$

where h is Planck's constant, υ is the photon frequency, E_g is the bandgap and α is the absorption coefficient obtained from the experimental transmission values (T) according to the expression below:[1]

$$\alpha = \frac{1}{d}\ln(\frac{1}{T}),$$

where d is the film thickness. The thicknesses of the ZnO and CeO_x layers, measured by profilometry, are around 25 and 20 nm, respectively.

By plotting the curve $(\alpha h\upsilon)^2$ as a function of incident photon energy ($h\upsilon$), the bandgap energy values E_g for ZnO and CeO_x were determined by linear extrapolation of the curve to the energy axis and found to be 3.5 eV and 3.55 eV, respectively.

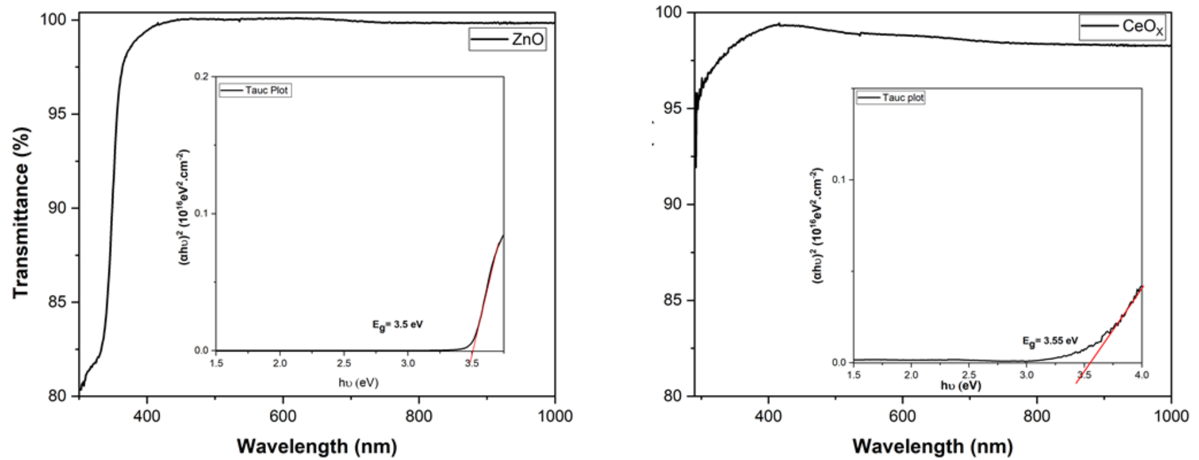

Figure S4. Transmission spectra of ZnO and CeO_x thin films on glass and determination of E_g.

4. Contact angle measurements

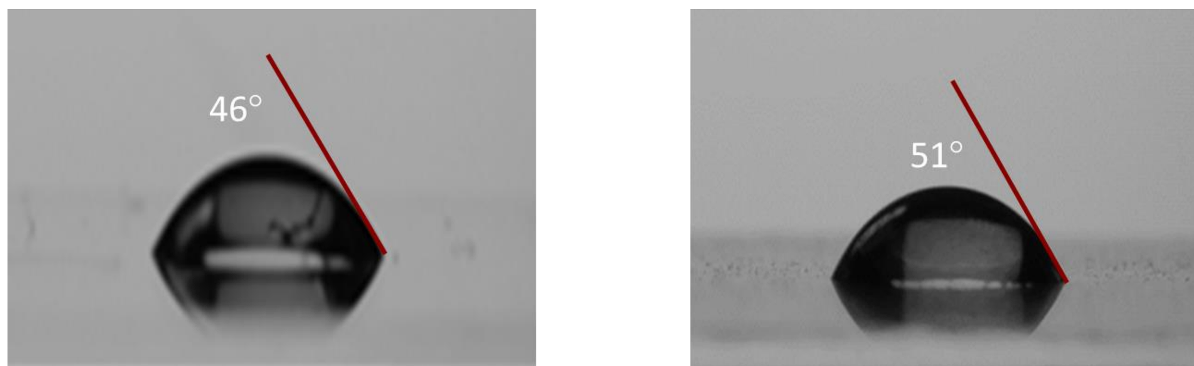

Figure S5. Contact angle measurements of a drop of water on a film of ZnO (left) and CeO_x (right).

5. Absorption spectra of the P3HT:PC_{61}BM photoactive layer

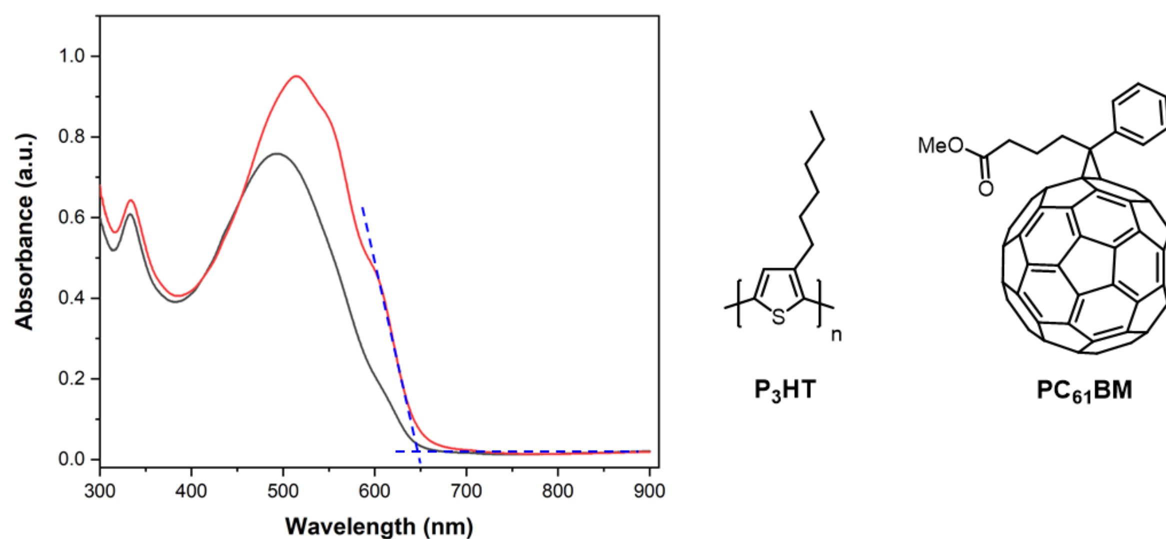

Figure S6. Absorption spectra of the P3HT:PC_{61}BM active layer on glass as spin-cast (black) and after annealing at 110°C for 3 minutes. Determination of the optical bandgap:
λ = 651 nm, E_g (eV) = (hc)/(eλ) = 1240/651 = 1.90 eV.

6. AFM analysis of the P3HT:$PC_{61}BM$ photoactive layer

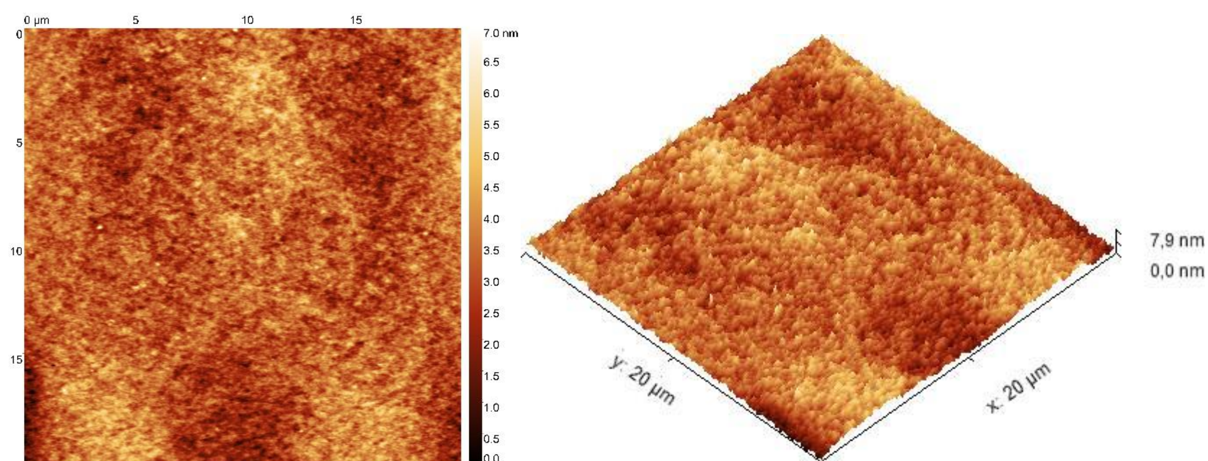

RMS = 0.76 nm

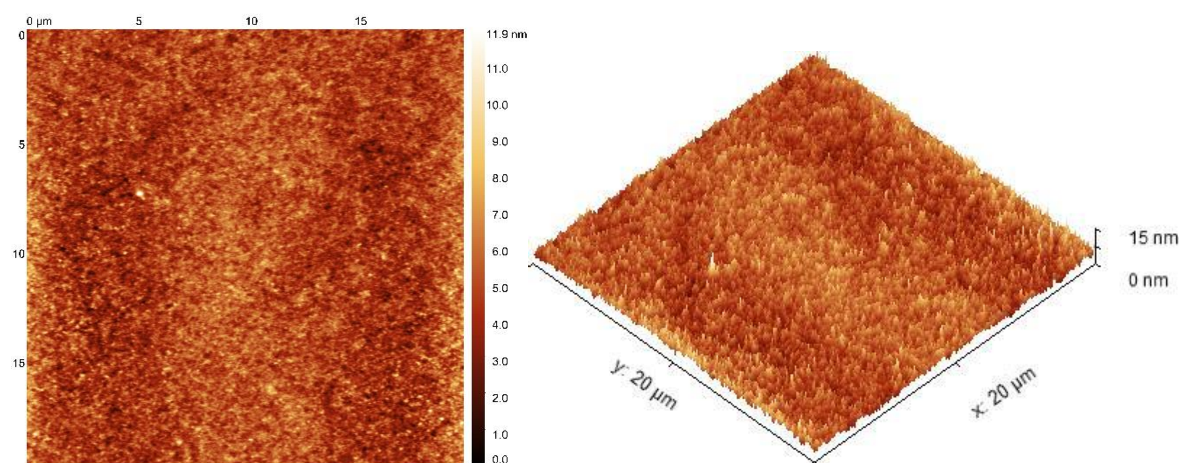

RMS = 2.86 nm

Figure S7. Contact mode AFM images of a P3HT:$PC_{61}BM$ layer before (Top) and after (Bottom) thermal annealing at 110°C for 3 minutes.

7. PESA measurements and determination of ionization energies

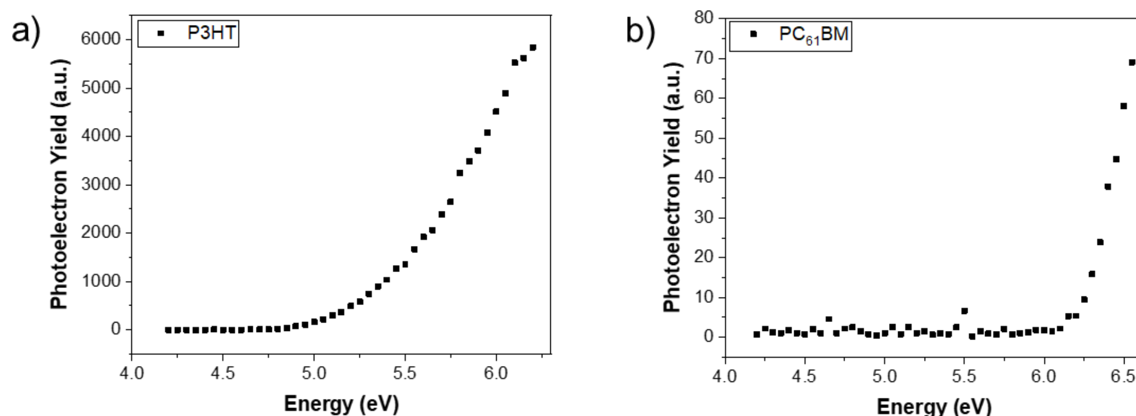

Figure S8. PESA spectra of thin films of P3HT (a) and $PC_{61}BM$ (b).

The ionization energy IE (HOMO energy) was determined through a fitting procedure based on data obtained from Photoelectron Spectroscopy in Air (PESA) measurements. This technique allowed for the precise estimation of IE by utilizing the following empirical model:

- For $V < IE$, the response function is constant, $Y = Y_0$.
- For $V \geq IE$, the response function is described by the equation $Y = Y_0 + a * (V - IE)^{(1/n)}$, where a is a scaling factor and n is an exponent characterizing the response curve, close to 0.5.

To validate the accuracy and robustness of the model, the data were plotted on a logarithmic scale on the Y-axis. This approach effectively highlights the consistency of the empirical model across different voltage ranges, confirming its reliability in estimating the ionization energy.

8. AFM analysis of CeO_x layers

CeO_x layers obtained after TA at 200°C for 15 min

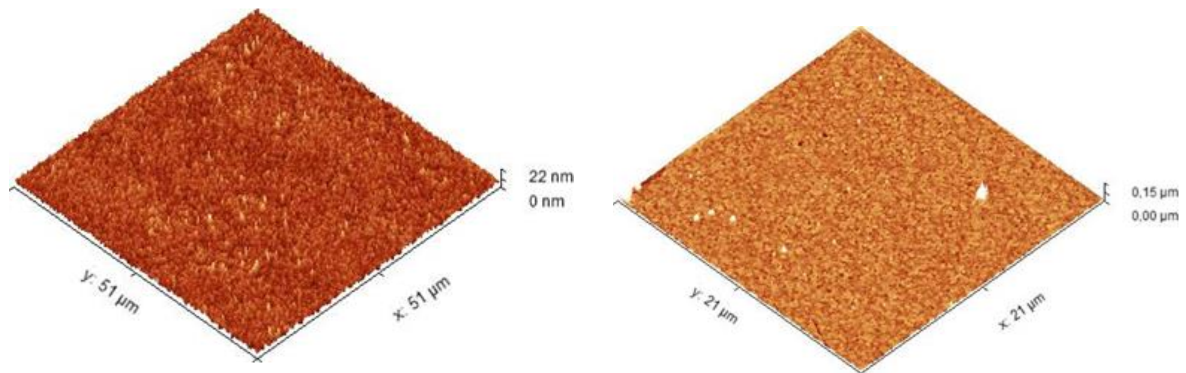

CeO_x layers obtained after TA at 450°C for 15 min

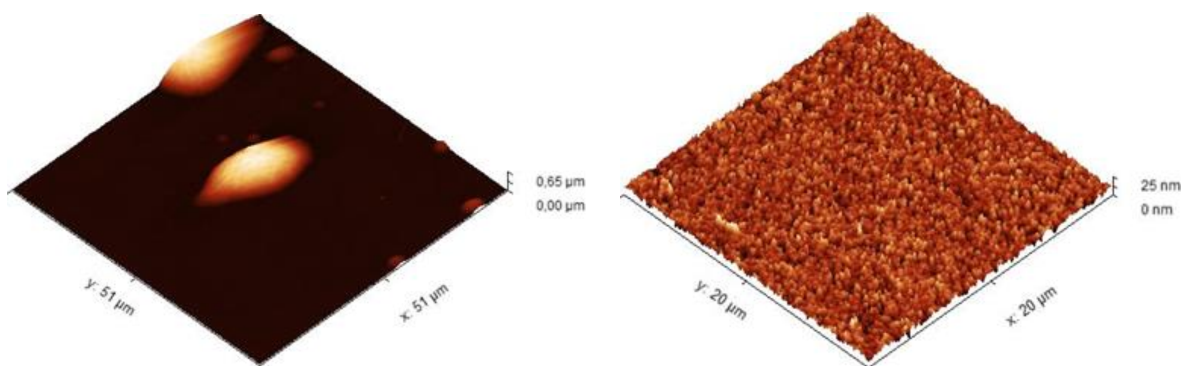

Figure S9. Contact mode AFM images (50 µm × 50 µm and 20 µm × 20 µm) of CeO_x films annealed for 15 min at 200°C (top) or 450°C (bottom).

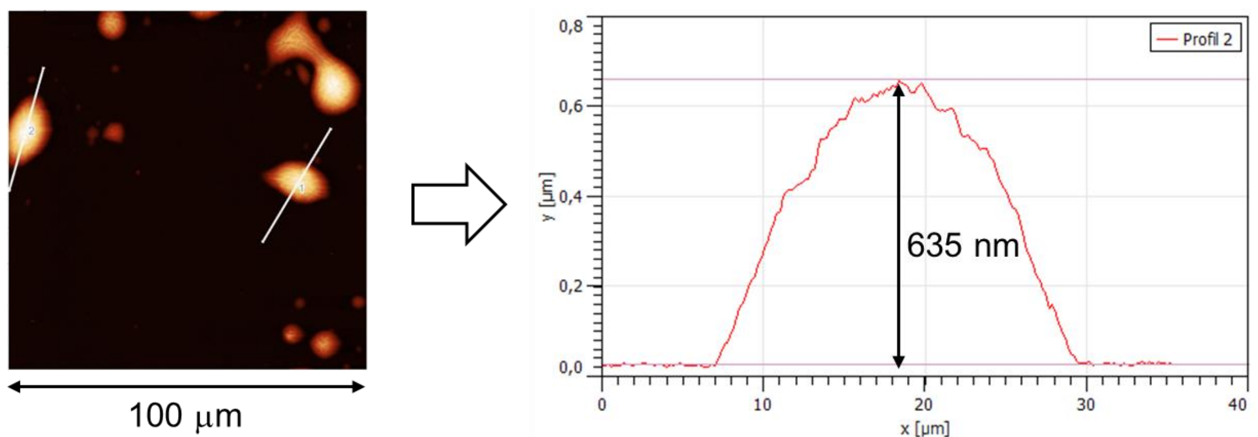

Figure S10. AFM images (100 µm ×100 µm) in contact mode of a CeO_x film annealed for 15 min at 450°C and profile of one crystalline cluster showing a height of 635 nm.

9. Evaluation of device stability

Conditions: The OPV devices were stored in a glove box under 2.5 mbar of argon in ambient light at 20°C, in the absence of organic solvents, with the amount of water and oxygen being less than 0.1 ppm for both.

Table S1. Photovoltaic efficiency of a ZnO-based device in a controlled atmosphere (Ar) as a function of time

Time (h)	J_{sc} (mA cm^{-2})	V_{oc} (V)	FF (%)	PCE (%)
T_0	9.48	0.56	56	3.00
48 h	9.42	0.56	57	3.05
168 h	9.54	0.57	58	3.16
384 h	9.22	0.57	58	3.07
720 h	9.04	0.57	59	3.05

Table S2. Photovoltaic efficiency of a CeO_x-based device in a controlled atmosphere (Ar) as a function of time

Time (h)	J_{sc} (mA cm^{-2})	V_{oc} (V)	FF (%)	PCE (%)
T_0	8.60	0.45	44	1.71
120 h	9.15	0.46	43	1.81
168 h	9.71	0.46	43	1.92
384 h	9.80	0.47	46	2.12
720 h	9.30	0.45	43	1.80

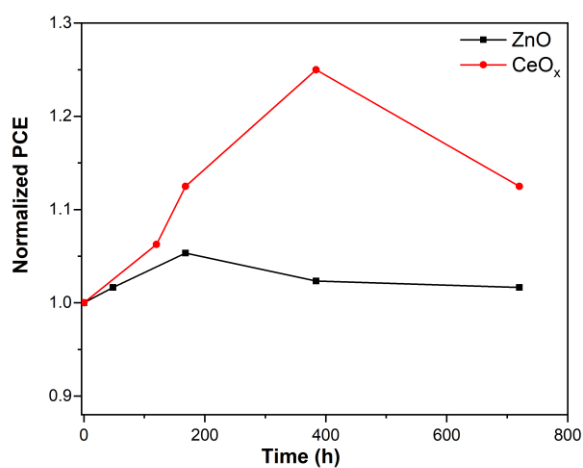

Figure S11. Photovoltaic efficiency of devices in a controlled atmosphere (Ar) as a function of time.

Table S3. Photovoltaic efficiency of a ZnO-based device in a controlled atmosphere (Ar) as a function of time (Note that ZnO was prepared from a different procedure than the previous one in Table S1)

Time (month)	J_{sc} (mA cm^{-2})	V_{oc} (V)	FF (%)	PCE (%)
T_0	9.03	0.56	53	2.65
1	8.21	0.55	55	2.49
5	7.23	0.53	53	2.01

Table S4. Photovoltaic efficiency of a device using the mixed ZnO/CeO_x layer in a controlled atmosphere as a function of time.

Time (month)	J_{sc} (mA cm^{-2})	V_{oc} (V)	FF (%)	PCE (%)
T_0	8.25	0.50	50	2.08
1	7.79	0.51	51	2.03
5	7.87	0.52	43	1.77

10. References

1. P. Nagaraju, Y. VijayaKumar, P. Radhika, R. J. Choudhary and M. V. RamanaReddy, *Materials Today: Proceedings*, 2016, **3**, 4009.